THE JOURNAL OF PHYSICAL CHEMISTRY C

Article

pubs.acs.org/JPCC

Hydrogen and Oxygen Evolution Photocatalysts Synthesized from Strontium Titanate by Controlled Doping and Their Performance in Two-Step Overall Water Splitting under Visible Light

Shoichi Hara,[†] Masaharu Yoshimizu,[†] Satoshi Tanigawa,[†] Lei Ni,[‡] Bunsho Ohtani,[§] and Hiroshi Irie*[,‡,∥]

[†]Special Educational Program on Clean Energy, Interdisciplinary Graduate School of Medicine and Engineering, University of Yamanashi, 4-3-11 Takeda, Kofu, Yamanashi 400-8511, Japan

[‡]Clean Energy Research Center, University of Yamanashi, 4-3-11 Takeda, Kofu, Yamanashi 400-8511, Japan

[§]Catalysis Research Center, Hokkaido University, Nishi 10, Kita 21-jyo, Kita-ku, Sapporo, Hokkaido 001-0021, Japan

[∥]Japan Science and Technology Agency, CREST, 5 Sanbancho, Chiyoda-ku, Tokyo 102-0075, Japan

Supporting Information

ABSTRACT: A visible-light-induced two-step overall water splitting was achieved by combining two types of photocatalysts prepared by introducing foreign elements into the identical mother structure with a controlled electronic band structure. Strontium titanate ($SrTiO_3$) was selected as the mother structure and was doped with either vanadium (and sodium) or rhodium to introduce visible light sensitivity. By utilizing these two types of $SrTiO_3$-based photocatalysts, simultaneous liberation of hydrogen (H_2) and oxygen (O_2) with a molar ratio of ∼2:1 was achieved in the presence of iodate ion (IO_3^-)/iodide ion (I^-) as a redox mediator under irradiation with only visible light (>420 nm).

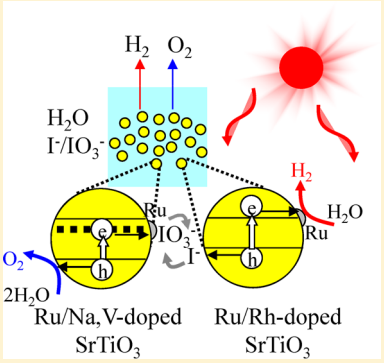

INTRODUCTION

Since the Honda−Fujishima effect was first reported regarding photoinduced water splitting by titanium dioxide (TiO_2) and platinum (Pt) electrodes, various photocatalytic materials have been investigated because the generated hydrogen (H_2) represents a clean and renewable fuel source.[1−4] Among examined materials, strontium titanate ($SrTiO_3$, hereafter STO) is a promising photocatalyst due to its high thermal stability and resistance to photocorrosion; however, STO powder alone cannot split water into H_2 and oxygen (O_2). In fact, Yoneyama et al.[5] reported that reduced STO powder could decompose water into H_2 and O_2 in stoichiometric amounts. They demonstrated that the rate of the decomposition showed a tendency to diminish with illumination time and attributed it to some change in the surface condition of the catalyst. Therefore, in general, the modification is necessary for STO to function as an active photocatalyst, evolving H_2 and O_2 in stoichiometric amounts linearly and catalytically. Notably, the nickel oxide modification of STO facilitates the UV-light-induced photocatalytic splitting of water into H_2 and O_2.[6,7] However, to increase the efficiency of solar energy utilization by STO, it is necessary to first improve its sensitivity to visible light.

To increase the visible light sensitivity of STO, numerous studies have employed the doping of foreign elements into the STO lattice. Following irradiation with visible light, doped STO is able to generate either H_2 or O_2 in the presence of a sacrificial agent, a process termed half water splitting.[8] In addition, combined systems consisting of doped STO, such as Pt-deposited chromium and tantalum-codoped or rhodium-doped STO as the H_2-production photocatalyst, and Pt-deposited tungsten trioxide or bismuth vanadate as the O_2-production photocatalyst, can function as visible-light-sensitive photocatalysts for overall water splitting in the presence of a suitable redox mediator (two-step overall water splitting).[9−11] Recently, Maeda et al. successfully created such a system using only tantalum oxynitride based photocatalysts.[12]

Here, we have achieved a two-step overall water splitting by combining only STO-based materials under irradiation with only visible light. To our knowledge, this is the first study to generate a visible-light-sensitive photocatalyst system through the introduction of foreign elements into the identical mother structure to control its electronic band structure. Very recently, we established a similar STO-based system; however, it required UV light irradiation.[13]

EXPERIMENTAL SECTION

Preparations. STO, sodium (Na) and vanadium(V) codoped STO ($(Sr_{0.99}Na_{0.01})(Ti_{0.99}V_{0.01})O_3$, Na,V-STO), and

Received: June 27, 2012
Revised: July 28, 2012
Published: July 30, 2012

rhodium (Rh)-doped STO ($Sr(Ti_{0.99}Rh_{0.01})O_3$, Rh-STO) were prepared as follows. STO was synthesized using a conventional solid-state reaction. Commercial $SrCO_3$ (Kanto Kagaku, purity 99.9%) and TiO_2 (High Purity Chemicals, purity 99.99%) powders were used as the starting materials. Stoichiometric amounts of the starting materials for STO were wet-ball-milled for 20 h using zirconium dioxide (ZrO_2) balls as the milling medium in polyethylene bottles. The resulting mixture was calcined at 1100 °C for 6 h and then thoroughly ground.

Na,V-STO was synthesized using a two-step solid-state reaction. In the first step, STO (identical procedure above) and sodium vanadate ($NaVO_3$, NVO) were synthesized by a conventional solid-state reaction. Stoichiometric amounts of the starting materials for NVO, sodium carbonate (Na_2CO_3, Kanto Kagaku, purity 99.8%), and vanadium oxide (V_2O_5, Kanto Kagaku, purity 99.0%) powders, were wet-ball-milled in the identical manner. The mixture for preparing NVO was calcined at 300 °C for 3 h and then thoroughly ground. The obtained powders were pressed into pellets, heated at 450 °C for 6 h, and then thoroughly ground to obtain NVO powders. To prepare Na,V-STO, stoichiometric amounts of the prepared STO and NVO powders were wet-ball-milled in the identical process. The resulting mixture was calcined at 550 °C for 6 h, below the melting temperature of NVO (600 °C), and then thoroughly ground. The obtained powders were pressed into pellets, heated 1100 °C for 6 h, and then thoroughly ground to obtain Na,V-STO powder.

Rh-STO was also synthesized using the solid-state reaction. Commercial $SrCO_3$ (the same as above), TiO_2 (the same as above), and rhodium oxide (Rh_2O_3, Kanto Kagaku, purity 99.9%) powders were used as the starting materials. Stoichiometric amounts of the starting materials for Rh-STO were wet-ball-milled identically. The resulting mixture was calcined at 1000 °C for 10 h and then thoroughly ground to obtain Rh-STO powder (Supporting Information, section S.I.1).

The deposition of the ruthenium (Ru) cocatalyst onto STO (Ru/STO), Na,V-STO (Ru/Na,V-STO), and Rh-STO (Ru/Rh-STO) and the platinum (Pt) cocatalyst onto STO (Pt/STO) was performed using a photodecomposition method.[14] Briefly, 0.5 g of STO, Na,V-STO, or Rh-STO powder was first dispersed in 80 mL of distilled water containing 20 mL of methanol. Ruthenium chloride ($RuCl_3 \cdot nH_2O$; n was assumed to be 3), which served as the source of Ru, was then weighed to give a weight fraction of Ru relative to STO, Na,V-STO, and Rh-STO of 5×10^{-4}, 5×10^{-4}, and 7×10^{-3}, respectively. The Pt source, hydrogen hexachloroplatinate (H_2PtCl_6), was then weighed to give a weight fraction of Pt relative to STO of 1×10^{-3}. Weighed $RuCl_3 \cdot nH_2O$ or H_2PtCl_6 was added to the aqueous sample suspension, which was then sufficiently deaerated using liquid nitrogen (N_2). After the deaeration of both Na,V-STO and Rh-STO, the suspensions were subjected to light irradiation for 4 h using a xenon (Xe) lamp (LA-251Xe, Hayashi Tokei) equipped with an optical filter (Y-44, Hoya). After the deaeration of STO, a Xe lamp without an optical filter was used for light irradiation of the suspension for 4 h. Each suspension was then filtered with a membrane filter (5−10 μm, Whatman) and washed with sufficient amounts of distilled water. Each of the resulting residues was dried at 80 °C for 24 h and then ground into a fine powder using an agate mortar and pestle.

Characterizations. Elemental analysis of the prepared photocatalysts (Ru/Na,V-STO and Ru/Rh-STO) was performed using an inductively coupled plasma atomic emission spectrometer (ICP-AES) (SPS1700, Seiko Instruments Inc.) for constituent elements. The crystal structures of the prepared powders were identified by X-ray diffraction (XRD) (Panarytical PW-1700). UV−visible (UV−vis) absorption spectra were obtained by the diffuse reflection method using a spectrometer (either UV-2550, Shimadzu or V-650, JASCO) and $BaSO_4$ as a reflectance standard. Surface composition was evaluated by X-ray photoelectron spectroscopy (XPS) (JPS-9200, JEOL).

Water-Splitting Reactions. *Action Spectrum Measurements.* H_2 and O_2 evolutions were observed in the presence of Ru/Rh-STO or Ru/Na,V-STO (30 mg each) with the aid of iodide ion (I^-) (sodium iodide (NaI), Kanto Kagaku, 0.01 mol/L) or iodate ion (IO_3^-) (sodium iodate ($NaIO_3$), Kanto Kagaku, 0.01 mol/L) as a sacrificial agent, respectively. The measurements were performed in 3 mL of water, without adjusting the pH of the solution, while stirring using a magnetic stirrer under monochromatic light (360 ± 5, 420 ± 5, 480 ± 5, 540 ± 5, and 600 ± 5 nm) using a diffraction grating-type illuminator (CRM-FD, JASCO) equipped with a 300-W xenon lamp (C2578-02, Hamamatsu Photonics). Higher-order diffracted light was cut off with the appropriate glass filter.

The H_2 evolution reaction in the presence of Pt/STO and I^- (0.01 mol/L) as a sacrificial agent was measured under monochromatic light using a Czerny-Turner type monochromator (MC-10N, Ritsu Ouyou Kogaku) and a Xe lamp (LA-251Xe, Hayashi Tokei). Monochromatic light with a wavelength of either 360 ± 10 or 420 ± 10 nm was used. Higher-order diffracted light was cut off with the appropriate glass filter.

The amounts of evolved H_2 and O_2 were monitored using a gas chromatograph (GC-8A, Shimadzu). The wavelength dependence of the apparent quantum efficiency (AQE) and quantum efficiency (QE) was then evaluated. The AQE values for H_2 and O_2 evolution were calculated using the equations, AQE (%) = 2 × H_2 evolution rate/incident photon rate ×100, and 4 × O_2 evolution rate/incident photon rate ×100, respectively, because H_2 and O_2 evolutions are represented by the formulas $2H^+ + 2e^- \rightarrow H_2$ and $2H_2O + 4h^+ \rightarrow O_2 + 4H^+$, respectively. When obtaining QE values, the absorption rate of incident photons was utilized instead of the incident photon rate.

Two-Step Overall Water-Splitting Measurements. Photocatalytic overall water-splitting tests were conducted in a gas-closed circulation system. Ru/Na,V-STO and Ru/Rh-STO powders (30 mg each) were mixed with I^- (0.01 mol/L) and IO_3^- (0.01 mol/L) as redox mediators and suspended in 10 mL of water using a magnetic stirrer. For reference, the identical test in the presence of bare Na,V-STO and Rh-STO powders (30 mg each) instead of Ru/Na,V-STO and Ru/Rh-STO powders (30 mg each) was conducted. The pH of the resulting suspension was not adjusted. However, it was measured using a pH meter (Automatic pH Titrator, DelsaNano AT, Beckman Coulter). Argon gas (50 kPa) was introduced into the system after repeated deaeration down to 2.5 Pa. A Xe lamp with an optical filter (Y-44, Hoya) was used for light irradiation (>420 nm). The reaction was allowed to proceed repeatedly with evacuation every 48 h. The amounts of evolved H_2 and O_2 were monitored using an online gas chromatograph (GC-8A, Shimadzu).

Half Water-Splitting Measurements. Photocatalytic half water-splitting tests were also conducted in a gas-closed circulation system. Either Na,V-STO, Rh-STO, Ru/STO, Ru/

Na, V-STO, or Ru/Rh-STO powder (60 mg each) was mixed with either IO_3^- (0.01 mol/L) or I^- (0.01 mol/L) as a sacrificial agent and suspended in 10 mL of water using a magnetic stirrer. A Xe lamp with an optical filter (the same) was used for light irradiation (>420 nm). The amounts of evolved H_2 and O_2 were monitored using an online gas chromatograph (the same).

RESULTS AND DISCUSSION

Characterizations of the Prepared Photocatalysts. Elemental analyses by ICP-AES indicated that the molar ratios of Na/Sr/V/Ti in Ru/Na,V-STO and Sr/Rh/Ti in Ru/Rh-STO were 0.0094:0.99:0.010:0.99 and 1.0:0.011:0.98, respectively, both of which were close to the starting ratios used in the preparation. In addition, the analyses indicated that the weight fractions of Ru relative to Na,V-STO and Rh-STO were 5.0×10^{-4} and 7.3×10^{-3}, respectively, in Ru/Na,V-STO and Ru/Rh-STO, nearly equal to the starting fractions used in the preparation. Na,V-STO was confirmed to have a single phase of cubic STO (Figure S1, section S.I.2, Supporting Information). Na and V ions were likely successfully incorporated at Sr and Ti sites, respectively, in Na,V-STO. Although Rh-STO included unknown impurity peaks in the X-ray diffraction (XRD) pattern, it appeared that a part of Rh ions were incorporated at a Ti site in Rh-STO (Figure S1, section S.I.2, Supporting Information).[15] The UV−visible absorption spectra of STO, Na,V-STO, and Rh-STO were obtained using a diffuse reflection method (Figure 1). For Na,V-STO, the formation

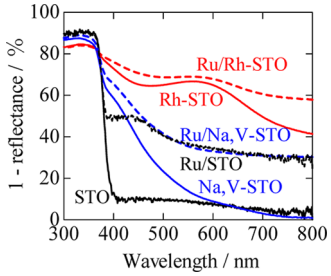

Figure 1. UV−visible absorption spectra of STO, Na,V-STO, Rh-STO, Ru/STO, Ru/Na,V-STO, and Ru/Rh-STO. After Ru deposition onto STO, Na,V-STO, and Rh-STO, increased absorption at a wider wavelength region (>400 nm) was observed.

of an absorption shoulder in the visible light region up to ~600 nm and a negligible shift of the absorption edges were observed. These findings indicate that the band gap of Na,V-STO was not narrowed from that of STO; however, an isolated mini-band composed of V 3d orbitals was formed in the forbidden band below the conduction band (CB), which was composed of Ti 3d orbitals.[13] It is noteworthy that the Na 2p orbitals contributed to neither the CB nor the valence band (VB). In this case, Na^+ at a Sr^{2+} site only acted as a counter dopant to V^{5+} at a Ti^{4+} site to maintain the charge neutrality in Na,V-STO. In contrast, absorption in the entire range of visible light was observed for Rh-STO, with a peak occurring at ~600 nm. According to Konda et al.,[16] the existence of two different doped Rh species (Rh^{3+} and an Rh species with a higher oxidation state than Rh^{3+}, such as Rh^{5+}) is responsible for this spectral pattern. The absorption with a peak occurring at ~600 nm originated from the higher oxidation state of the Rh species, and the one with the shorter wavelength region from Rh^{3+}. In this system, the Rh species with a higher oxidation state is easily reduced to Rh^{3+} by photogenerated electrons. More importantly, Konda et al.[16] asserted that the band gap of $Sr(Ti_{0.99}Rh_{0.01})O_3$ (i.e., Rh-STO in the present study) is narrowed by the partial overlap of Rh $4d^6$ (Rh^{3+}) and O 2p orbitals to form the VB, resulting in a negative-potential shift of the VB top, which will be discussed later. In the spectra of Ru/STO, Ru/Na,V-STO, and Ru/Rh-STO (Figure 1), the absorption over a wider wavelength region (>400 nm) clearly increased because Ru was deposited onto STO, Rh-STO, and Na,V-STO powders.

The XPS spectra for Ru 3d and Pt 4f were also recorded. The metallic form of either Ru^0 (Ru $3d_{5/2}$ at ~281 eV)[17] in Ru/STO, Ru/Na,V-STO, and Ru/Rh-STO or Pt^0 (Pt $4f_{7/2}$ and Pt $4f_{5/2}$ at ~70 and ~73 eV, respectively)[18] in Pt/STO was also confirmed (Figure S2a,b, section S.I.3, Supporting Information). Note that the XPS peak at ~198 eV, derived from Cl (Cl $2p_{3/2}$),[19] was not observed in Ru/STO, Ru/Na,V-STO, Ru/Rh-STO, and Pt/STO at all, whereas it was observed in the mechanical mixture of STO and $RuCl_3 \cdot nH_2O$ (n was assumed to be 3; weight fraction of Ru relative to STO was 5.0×10^{-4}) and in that of STO and H_2PtCl_6 (weight fraction of Pt relative to STO of 1.0×10^{-3}) (Figure S2c, section S.I.3, Supporting Information). This indicates that the prepared photocatalysts are free from Cl ions even though either Ru- or Pt-chloride was used as the source of Ru or Pt.

Water-Splitting Reactions. Figure 2a shows the action spectrum[20] for O_2 evolution from an aqueous IO_3^- solution

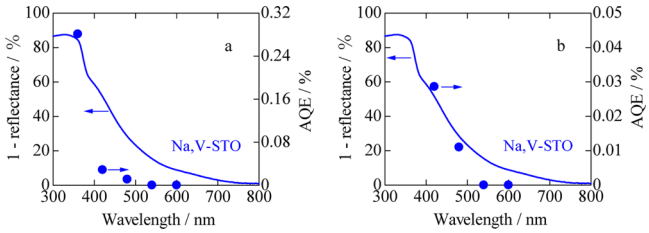

Figure 2. (a) Action spectrum for O_2 evolution from an aqueous IO_3^- solution over Ru/Na,V-STO accompanied by the UV−visible absorption spectrum of Na,V-STO. (b) Enlargement of (a).

over the Ru/Na,V-STO photocatalyst. Ru/Na,V-STO was able to utilize visible light up to ~500 nm, although the apparent quantum efficiency (AQE) values in the visible light range did not coincide with those of the UV−visible spectrum when the one in the UV range (360 nm) was adjusted to coincide with it. In contrast, the AQE values in the visible light range (420−480 nm) coincided well with the UV−visible spectrum unless the one in the UV range (360 nm) was adjusted to coincide with it. Moreover, the AQE value at 360 nm was 1 order of magnitude larger than those at 420 and 480 nm, a response that was likely due to differences in the QE values resulting from irradiation with UV and visible lights. In fact, QE values under irradiation with 360 nm UV light and 420 and 480 nm visible light were 0.33, 0.056, and 0.039%, respectively. Even when Ru/Na,V-STO was irradiated with visible light, QE values decreased with increasing wavelength of irradiating light. These observations clearly support the formation of an isolated mini-band in Na,V-STO (section S.I.4, Supporting Information),[21−23] as discussed above. Although Na,V-STO could absorb visible light up to ~700 nm, the AQE values for this photocatalyst at 540 and 600 nm were zero. This phenomenon, which is frequently encountered in oxygen-defective photocatalysts,[21,24] is plausible when we consider that visible absorption between ~540 and

dx.doi.org/10.1021/jp306315r | J. Phys. Chem. C 2012, 116, 17458−17463

700 nm originated from the oxygen deficiency of Na,V-STO, even though Na was utilized as the counter dopant to maintain charge neutrality and avoid the generation of oxygen defects.

In the action spectrum for H_2 evolution from an aqueous I^- solution over the Ru/Rh-STO photocatalyst (Figure 3), it was

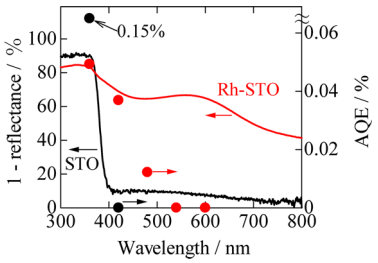

Figure 3. Action spectra for H_2 evolution from an aqueous I^- solution over Ru/Rh-STO (red circles) and Pt/STO (black circles) accompanied by UV−visible absorption spectra of STO (black line) and Rh-STO (red line).

confirmed that Ru/Rh-STO was able to utilize visible light up to ∼500 nm. Importantly, the AQE values for this material under irradiation with UV (360 nm) and visible light (420 nm) coincided well with the UV−visible spectrum of Rh-STO. This observation indicates that Rh-STO experienced band gap narrowing, which was different from the case of Na,V-STO (section S.I.4, Supporting Information), a finding that coincided with that of Konda et al.,[16] as discussed above. The QE values for H_2 evolution when irradiated with 360 and 420 nm light were similar at 0.059% and 0.054%, respectively.[22,24,25] Here, the AQE value at 480 nm decreased and shifted away from the UV−visible spectrum of Rh-STO, while the values at 540 and 600 nm were reduced to zero (Figure 3). These findings also support the conclusions of Konda et al.,[16] who stated that Rh-STO contains Rh species with different oxidation states; the Rh species with a higher oxidation state is responsible for absorption of the peak wavelength of ∼600 nm and can be easily converted to Rh^{3+} upon irradiation with light. Thus, absorption with a peak occurring at ∼600 nm does not contribute to the photocatalytic activity of Rh-STO.

The spectrum for H_2 evolution from the aqueous NaI solution over Pt-deposited STO (Pt/STO) was also measured (Figure 3). Because of the 3.2 eV band gap of STO, it is reasonable that STO was active (AQE = 0.15%) when irradiated with monochromic UV light (360 nm), but was inactive upon irradiation with visible light (420 nm).

We examined water splitting over Ru/Rh-STO and Ru/Na,V-STO, utilizing IO_3^-/I^- as a redox mediator (the pH of the suspension was measured to be 8.6), under irradiation with visible light (>420 nm) for 144 h with evacuation of the system every 48 h (Figure 4). As shown in Figure 4a, and Figure S3a in section S.I.5 in the Supporting Information, H_2 and O_2 were evolved in a linear manner with increasing irradiation time. In addition, both molecules were evolved at similar levels during each irradiation cycle. More importantly, the ratio of evolved H_2 to O_2 was nearly stoichiometric (∼2 to 1) in every cycle (Figure 4b). This result demonstrates that overall water splitting in this system was achieved. In contrast, over bare Rh-STO and Na,V-STO utilizing IO_3^-/I^- as a redox mediator under irradiation with visible light (>420 nm), only O_2 was evolved (Figure 4a, and Figure S3b in section S.I.5, Supporting Information), whereas H_2 was not evolved at all. The O_2 evolution was attributable to the half water splitting, caused by

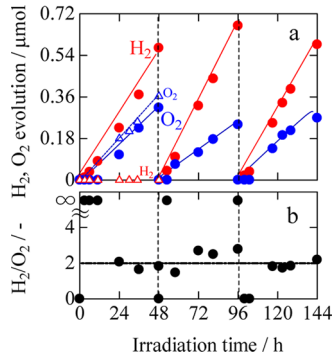

Figure 4. (a) Time courses of H_2 and O_2 (closed circles) evolution resulting from water splitting in the presence of Ru/Na,V-STO and Ru/Rh-STO photocatalysts irradiated with visible light (>420 nm). The reaction was allowed to proceed for 144 h with evacuation every 48 h. In the first period up to 48 h, those of H_2 and O_2 (triangles) evolution in the presence of bare Na,V-STO and Rh-STO irradiated with visible light (>420 nm) are plotted. (b) Ratio of evolved H_2 to O_2 in the presence of Ru/Na,V-STO and Ru/Rh-STO obtained from the data in (a). When only H_2 was detected in the initial period of the cycle, the ratio was indicated as ∞.

bare Na,V-STO as the O_2 evolution photocatalyst and IO_3^- as the sacrificial agent, which will be indicated in Figure 5a. The smaller O_2 evolution over Ru/Rh-STO and Ru/Na,V-STO than over bare Rh-STO and Na,V-STO is presumably caused by the reverse reaction to form H_2O from H_2 and O_2, resuting in the low O_2 amounts, because we could exclude the possibility to generate O_2 caused by bare Rh-STO with the aid of IO_3^-. According to Konda et al.,[16] Ru/Rh-STO could not evolve O_2 even with the aid of Ag^+, so it could be reasonable to consider that bare Rh-STO cannot evolve O_2 in the presence of IO_3^-. In contrast, bare Rh-STO could scarcely evolve H_2 even in the presence I^- as the sacrificial agent, as shown in Figure 5b.

Finally, we examined the evolutions of O_2 over Ru/Na,V-STO, bare Na,V-STO, and Ru/STO utilizing IO_3^- as a sacrificial agent in Figure 5a and those of H_2 over Ru/Rh-STO, Rh-STO, and Ru/STO utilizing I^-, under irradiation with visible light (>420 nm) in Figure 5b (Figure S4a−f in section S.I.5, Supporting Information). As shown in Figure 5a, the O_2 evolution proceeded over Ru/Na,V-STO and bare Na,V-STO in the presence of IO_3^-. It is quite natural that the O_2 evolution rate was larger over Ru/Na,V-STO than over bare Na,V-STO as Ru acts as the cocatalyst. Although we could not figure out whether the observed O_2 over Ru/STO was originated from the splitting of H_2O or the contaminants (from either intruded air from the atomospheric condition or remaining O_2 in H_2O), the amounts of O_2 were so small. The amounts of H_2 were also plotted in Figure 5a, indicating that all of them were completely zero. Thus, we could confidently conclude that the introduced V 3d orbital was responsible for the O_2 evolution, not for the H_2 evolution, irradiated with visible light with the aid of IO_3^-. It is speculated that the cocatalyst Ru on Na,V-STO might be the active site for reducing IO_3^-, rather than for producing O_2.

As shown in Figure 5b, the H_2 evolution proceeded over Ru/Rh-STO, the negligibly small amount of H_2 was observed over bare Rh-STO, and H_2 evolution was not observed at all over Ru/STO in the presence of I^-. The amounts of O_2 were also plotted in Figure 5b. In some cases, negligibly small amounts of O_2 were detected; however, those were possibly originated from the contaminants from either intruded air or remaining O_2 in H_2O (Figure S4d−f in section S.I.5, Supporting

dx.doi.org/10.1021/jp306315r | J. Phys. Chem. C 2012, 116, 17458−17463

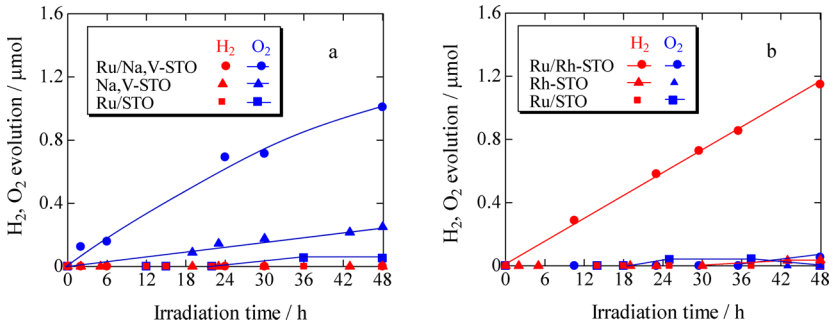

Figure 5. (a) Time courses of O_2 evolution resulting from half water splitting with the aid of IO_3^- sacrificial agent over Ru/Na,V-STO, bare Na,V-STO, and Ru/STO photocatalysts irradiated with visible light (>420 nm). In addition, plots of H_2 concentration were also included. However, H_2 concentrations in all cases were completely zero. (b) Time courses of H_2 evolution with the aid of I^- over Ru/Rh-STO, bare Rh-STO, and Ru/STO photocatalysts irradiated with visible light (>420 nm). In addition, plots of O_2 concentration were also included. When either H_2 or O_2 gas was detectable, plots were indicated with a line. In contrast, either H_2 or O_2 gas was not observed at all; plots were indicated without a line.

Information). Thus, we could confidently conclude that the introduced Rh 4d orbital was responsible for the H_2 evolution, not for the O_2 evolution, irradiated with visible light with the aid of I^-. More importantly, in the case of Rh-STO, the cocatalyst Ru on Rh-STO can be considered as the active site for H_2 evolution.

The stability of Ru/Na,V-STO and Ru/Rh-STO photocatalysts under visible light irradiation (>420 nm) was confirmed using XPS. Each of the photocatalysts after 48 h light irradiation in Figure 5a,b was collected and served for the measurements. Neither Sr 3d, Ti 2p, O 1s, Na 1s, V 2p, Rh 3d nor Ru 3d XPS spectra were changed after visible light irradiation (Figure S5a,b in section S.I.6, Supporting Information). Therefore, the present Ru/Na,V-STO and Ru/Rh-STO were quite stable under the present visible light condition.

As indicated above, (1) H_2 was linearly evolved when constructing the two-step water-splitting system over Ru/Na,V-STO and Ru/Rh-STO in Figure 4a, (2) H_2 was not evolved at all when constructing the system over bare Na,V-STO and Rh-STO in Figure 4a, and (3) H_2 was evolved with the aid of I^- sacrificial agent over Ru/Rh-STO (but scarcely over bare Rh-STO) in Figure 5b; so we can regard the cocatalyst Ru on Rh-STO as the main active-site for H_2 evolution in the two-step water-splitting system. Thus, we calculated the turnover number of generated H_2 to the total number of cocatalyst Ru to be ~1.2, indicating that this reaction proceeded catalytically (Figure S6 in section S.I.7, Supporting Information).

Taking these observations into consideration, the observed overall water splitting by Ru/Na,V-STO and Ru/Rh-STO (Figure 4a) irradiated with visible light was predominantly attributed to the introduced V 3d and Rh 4d states in the electronic band structure of STO. Particularly, Ru/Na,V-STO and Ru/Rh-STO contributed O_2 and H_2 with the aid of IO_3^- and I^-, respectively. In addition, it is reasonable to consider that Ru/Na,V-STO cannot evolve H_2 under visible light in the presence of I^- because the introduced V 3d state potential (presumably ~0.6 V) lies much more positive than the potential of H^+/H_2, allowing thermodynamically unfavorable H_2 evolution (Figure S7 in section S.I.8, Supporting Information). According to Konda et al.,[16] O_2 was not evolved at all under visible light over Ru/Rh-STO even in the presence of Ag^+, so it would be reasonable to consider that Ru/Rh-STO cannot evolve O_2 under visible light in the presence of IO_3^-. Taken together, we propose the possible mechanism for the overall water splitting by Ru/Na,V-STO and Ru/Rh-STO (Figure 4a), as schematically illustrated in Figure 6. Visible-light-excited electrons in the CB of Rh-STO are thought to

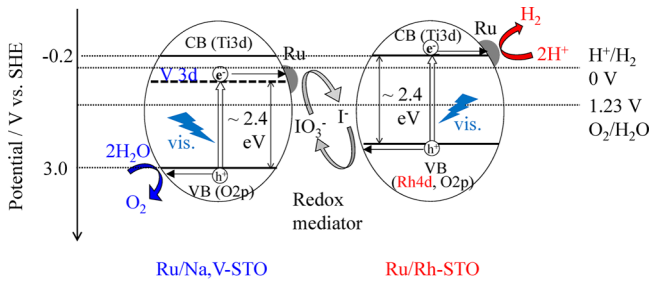

Figure 6. Schematic illustration of spontaneous H_2 and O_2 evolution by Ru/Na,V-STO and Ru/Rh-STO under irradiation with visible light in the presence of IO_3^-/I^- redox mediator.

reduce H_2O and generate H_2, and holes in the VB of Na,V-STO oxidize H_2O and produce O_2. In contrast, visible-light-excited holes in the VB of Rh-STO and electrons in the isolated V 3d state contribute to the turnover of I^- to IO_3^-, respectively, and vice versa.

CONCLUSIONS

We have established a two-step overall water-splitting system that is sensitive to visible light by utilizing two types of STO-based photocatalysts that simultaneously evolve H_2 and O_2 at a molar ratio of ~2 to 1 in the presence of IO_3^-/I^-. However, it is necessary to further enhance the visible light sensitivity. This will require the preparation of these STO-based photocatalysts hydrothermally in order to obtain deficient-free (O site in Na,V-STO), more highly crystallized, and smaller-sized particles. These investigations are currently being conducted in our laboratory. Moreover, as the band gap and band structure of STO are similar to those of TiO_2, it may be possible to construct a two-step overall water-splitting system utilizing TiO_2-based photocatalysts using the same strategy. The construction of such a system may be advantageous because TiO_2-based photocatalysts are nontoxic, stable, and naturally abundant, properties that are expected to facilitate their use in industrial and practical applications. Notably, we have achieved the simultaneous evolution of H_2 and O_2 under visible light using two types of TiO_2-based photocatalysts; the details will be reported elsewhere.

dx.doi.org/10.1021/jp306315r | J. Phys. Chem. C 2012, 116, 17458−17463

■ ASSOCIATED CONTENT

Supporting Information

Sample preparations, XRD, XPS, explanation of the band structures, raw data of N_2 and O_2 observations, stability of the photocatalysts, turnover number, and plots of Kubelka–Munk function. This material is available free of charge via the Internet at http://pubs.acs.org.

■ AUTHOR INFORMATION

Corresponding Author

*Tel: +81-55-220-8092. Fax: +81-55-220-8092. E-mail: hirie@yamanashi.ac.jp.

Notes

The authors declare no competing financial interest.

■ ACKNOWLEDGMENTS

This study was partially supported by the Cooperative Research Program of Catalysis Research Center, Hokkaido University (Grant No. 11C3002). We express gratitude to Mr. G. Newton for the careful reading of the manuscript.

■ REFERENCES

(1) Fujishima, A.; Honda, K. *Nature* **1972**, *238*, 37–38.
(2) Sato, J.; Saito, N.; Nishiyama, H.; Inoue, Y. *J. Phys. Chem. B* **2001**, *105*, 6061–6063.
(3) Kato, H.; Asakusa, K.; Kudo, A. *J. Am. Chem. Soc.* **2003**, *125*, 3082–3089.
(4) Maeda, K.; Teramura, K.; Lu, D.; Takata, T.; Saito, N.; Inoue, Y.; Domen, K. *Nature* **2006**, *440*, 295.
(5) Yoneyama, H.; Koizumi, M.; Tamura, H. *Bull. Chem. Soc. Jpn.* **1979**, *52*, 3449–3450.
(6) Domen, K.; Kudo, A.; Onishi, T.; Kosugi, N.; Kuroda, H. *J. Phys. Chem.* **1986**, *90*, 292–295.
(7) Domen, K.; Kondo, J. N.; Hara, M.; Takata, T. *Bull. Chem. Soc. Jpn.* **2000**, *73*, 1307–1331.
(8) Kato, H.; Kudo, A. *J. Phys. Chem. B* **2002**, *106*, 5029–5034.
(9) Sayama, K.; Mukasa, K.; Abe, R.; Abe, Y.; Arakjawa, H. *J. Photochem. Photobiol., A* **2002**, *148*, 71–77.
(10) Kato, H.; Sasaki, Y.; Iwase, A.; Kudo, A. *Bull. Chem. Soc. Jpn.* **2007**, *80*, 2457–2464.
(11) Kudo, A. *Int. J. Hydrogen Energy* **2007**, *32*, 2673–2678.
(12) Maeda, K.; Abe, R.; Domen, K. *J. Phys. Chem. Lett.* **2011**, *115*, 3057–3064.
(13) Hara, S.; Irie, H. *Appl. Catal., B* **2012**, *115–116*, 330–335.
(14) Tabata, S.; Nishida, H.; Masaki, Y.; Tabata, K. *Catal. Lett.* **1995**, *34*, 245–249.
(15) Iwase, A.; Ng, Y. H.; Ishiguro, Y.; Kudo, A.; Amal, R. *J. Am. Chem. Soc.* **2011**, *133*, 11054–11057.
(16) Konda, R.; Ishii, T.; Kato, H.; Kudo, A. *J. Phys. Chem. B* **2004**, *108*, 8992–8995.
(17) Hamzah, N.; Nordin, N. M.; Nadzri, A. H. A.; Nik, Y. A.; Kassim, M. B.; Yarmo, M. A. *Appl. Catal., A* **2012**, *419–420*, 133–141.
(18) Huang, B.-S.; Chang, F.-Y.; Wey, M.-Y. *Int. J. Hydrogen Energy* **2012**, *35*, 7699–7705.
(19) Irie, H.; Kamiya, K.; Shibanuma, T.; Miura, S.; Tryk, D. A.; Yokoyama, T.; Hashimoto, K. *J. Phys. Chem. C* **2009**, *113*, 10761–10766.
(20) Ohtani, B. *Chem. Lett.* **2008**, *37*, 217–229.
(21) Irie, H.; Watanabe, Y.; Hashimoto, K. *J. Phys. Chem. B* **2003**, *107*, 5483–5486.
(22) Irie, H.; Maruyama, Y.; Hashimoto, K. *J. Phys. Chem. B* **2007**, *111*, 1847–1852.
(23) Yan, X.; Ohno, T.; Nishijima, K.; Abe, R.; Ohtani, B. *Chem. Phys. Lett.* **2006**, *429*, 606–610.
(24) Takimoto, Y.; Kitta, T.; Irie, H. *Int. J. Hydrogen Energy* **2012**, *37*, 134–138.
(25) Qiu, X.; Miyauchi, M.; Yu, H.; Irie, H.; Hashimoto, K. *J. Am. Chem. Soc.* **2010**, *132*, 15259–15267.